

AI-assisted hyper-dimensional broadband quantum memory with efficiency above 90% in warm atoms

Zeliang Wu¹, Jinxian Guo^{2†}, Zhifei Yu³, Wenfeng Huang¹,
Chun-Hua Yuan^{1†}, Weiping Zhang², L.Q. Chen^{1†}

¹State Key Laboratory of Precision Spectroscopy, Quantum Institute for Light and Atoms, Department of Physics and Electronic Science, East China Normal University, Shanghai 200062, China.

²School of Physics and Astronomy, and Tsung-Dao Lee Institute, Shanghai Jiao Tong University, Shanghai 200240, China.

³School of Physics, Hefei University of Technology, Hefei, Anhui 230009, China.

Contributing authors: jxguo@sjtu.edu.cn; chyuan@phy.ecnu.edu.cn;
lqchen@phy.ecnu.edu.cn;

†These authors contributed equally to this work.

Abstract

High-dimensional broadband quantum memory significantly expand quantum information processing capabilities, but the memory efficiency becomes insufficient when extended to high dimensions. We demonstrate an efficient quantum memorize for hyper-dimensional photons encoded with orbital angular momentum (OAM) and spin angular momentum (SAM). OAM information is encoded from -5 to +5, combined with spin angular momentum encoding, enabling up to 22 dimensions. To ensure high memory efficiency, an artificial intelligent algorithm, a modified Differential Evolution (DE) algorithm using Chebyshev sampling, is developed to obtain a perfect signal-control waveform matching. Memory efficiency is experimentally achieved 92% for single-mode Gaussian signal, 91% for information dimension of 6 and 80% for dimensional number to 22. The fidelity is achieved up to 99% for single-mode Gaussian signal, 96% for OAM information and 97% for SAM one, which is far beyond no-cloning limitation. Our results demonstrate superior performance and potential applications in high-dimensional quantum information processing. This achievement provides a crucial foundation for future quantum communication and quantum computing.

Keywords: quantum memory, artificial intelligent algorithm, orbital angular momentum, quantum information

1 Introduction

As the demand for distributed quantum computing [1–4] and long-distance quantum communication [5–7] grows, the requirement for high data throughput has become increasingly urgent in quantum networks [8, 9]. High-dimensional broadband quantum memory is the performance metric for the scalability and effectiveness of quantum networks, ensuring they can support the high throughput demanded by the evolving quantum landscape. A 50% efficiency is the baseline for functionality, surpassing the 90% threshold is crucial for practical application in quantum networks.

So far, many high-dimensional and broadband quantum states have been generated in high-dimensional spaces across various domains, such as time [10], spatial mode [11], and spectrum [12–15] used for transmitting information. However, the efficiency of quantum memories remains a critical challenge, especially when scaling up to high dimensions and high bandwidths. Quantum state encoding the orbital angular momentum (OAM) is a typical high-dimensional quantum field. Memories of OAM light have been demonstrated with the bandwidth below MHz level [16, 17], they exhibit a significant drop in efficiency with higher topological charges. The efficiency for an OAM state with a topological charge of $l = 1$ reaches 70% [18], but it decreases to 60% for $l = 12$, highlighting the challenge of scaling efficiency with higher dimensions. While broadband quantum memories have been demonstrated with a bandwidth of 77 MHz and an efficiency of up to 82% for only single-mode Gaussian signals [19]. Quantum memory integrating high efficiency, high dimensional, and broadband is still a challenge in the field of quantum information science.

In this article, we experimentally demonstrate efficient hyper-dimensional broadband quantum memory in an ^{87}Rb atomic vapor cell using a far off-resonant Raman memory. To ensure high memory efficiency and high fidelity, an artificial intelligence (AI) technology, a modified DE algorithm based on Chebyshev sampling, is developed to enhance the manipulation accuracy of controlling waveform. With the assistance of DE algorithm, memory efficiency is achieved up to 92% and fidelity is 99% when the signal is a single-photon-level coherent optical pulse with the single-mode Gaussian (SMG) mode and bandwidth up to 50MHz. Then, OAM and spin angular momentum (SAM) are simultaneously encoded on the broadband signal to obtain hyper-dimensional information. AI-assisted signal-control waveform matching technology results in memory efficiency of 91% for dimensionality up to 6 and gradually decrease to 80% when dimensionality to 22. The fidelity reaches 96% and 97% for the OAM and SAM information, and can above the no-cloning limitation when the memory times are 1.0 μs and 50 μs , respectively. The results meet the practical requirements of quantum memory, laying a solid technical foundation for large-scale and high-speed quantum networks.

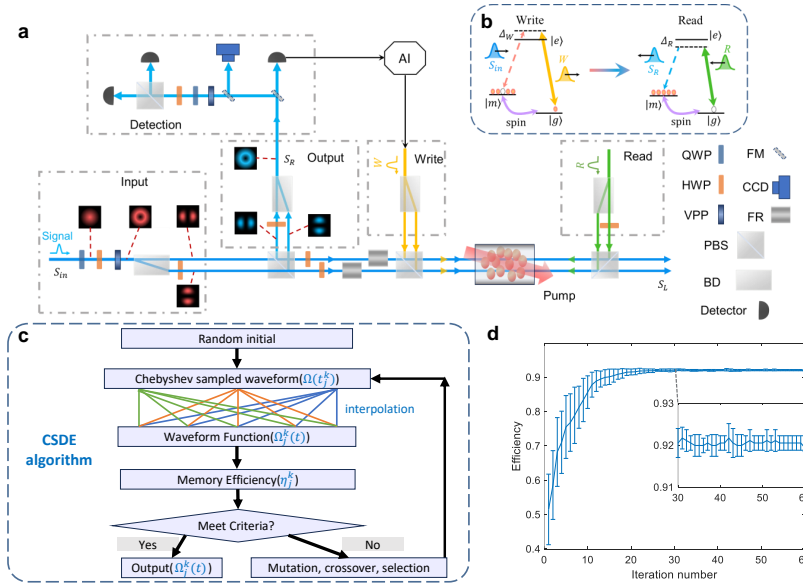


Fig. 1 Quantum memory scheme. (a) Experimental setup. VPP: vortex phase plate; HWP: half-wave plate; QWP: quarter-wave plate; BD: beam displacer; FR: Faraday rotator; FM: Flip mirror; PBS: polarization beam splitter; Rb cell: ^{87}Rb atomic vapor cell. W : write pulse; R : read pulse; S_{in} : input signal; S_L : leaked signal; S_R : retrieved signal. The intensities of the W/R beam is 270mW and 180mW, respectively. The pump and input signal are 50 μs and 20ns long, respectively. (b) Atomic energy level and light frequencies. $|g\rangle$: $|5^2S_{1/2}, F=1\rangle$ and $|m\rangle$: $|5^2S_{1/2}, F=2\rangle$ are the two hyperfine ground states of ^{87}Rb D_1 -line; $|e\rangle$: $|5^2P_{1/2}, F=2\rangle$ is the excited state; the detuning frequencies of S_{in} and R lights are $\Delta_W = 1.8\text{GHz}$ and $\Delta_R = -1.7\text{GHz}$, respectively. S_{in} and W satisfy two-photon resonant condition. (c) The flowchart of AI algorithm, that is, Chebyshev sampling differential evolution (CSDE) algorithm. The waveform of W is optimized via AI algorithm. (d) Efficiency as a function of the iteration number of AI algorithm. Memory efficiency is the ratio of the average photon number of S_R to that of S_{in} .

2 Results

2.1 Experimental setup

To efficiently memory hyper-dimensional information, it is necessary to be able to coherently store and retrieve OAM spatial modes and SAM polarization modes in the signal with efficiency above 90% and fidelity beyond no-cloning limitation. Here, we experimentally demonstrate the memory ability of spatial and polarization information of current memory system. The experimental diagram is given in Fig. 1a. A ^{87}Rb atomic vapor cell with a length of 7.5cm and a diameter of 2.5cm is placed inside a cylindrical magnetic shielding to reduce the influence of surrounding magnetic fields. The atomic energy level is shown in Fig. 1b. The atomic cell without buffer gas and anti-relaxation coating is heated to 84°C to achieve sufficient optical depth. Before write-in process, most atoms are populated on the atomic level of $|m\rangle$ by the pump pulse. The 20ns-long signal beam, signed as S_{in} is spatially overlapped with the strong write beam (W) by a polarizing beam splitter (PBS), and then enters into the atomic cell. S_{in} is partially stored as the spin excitation S_a with write-in efficiency η_W driven

by the W pulse. The rest signal is leaked out of the atoms as S_L . After some delay time τ , the atomic excitation can be retrieved back as readout optical signal (S_R) by a strong read pulse (R) in the backward direction. S_R and S_{in} are spatially overlapped and split using Faraday rotator, half-wave plate and polarized beam splitter as Fig. 1a shown. Finally, S_R is detected and analyzed by the detection system.

Temporal waveform of the S_{in} and S_R signals and memory efficiency can be measured using the photo-detector. The single-mode Gaussian signal carries OAM and SAM information after passing the vortex phase plate (VPP) and wave plates (half-wave plate, HWP and quarter-wave plate, QWP), respectively. The OAM signal is a superposition of Laguerre-Gaussian (LG) modes with different OAMs and with the radial index $p = 0$ [20], which can be written as $LG_l(r, \phi, z) = E_l(r, \phi, z) \exp(il\phi)$. ϕ is the azimuthal angle in the transverse plane, and l is the topological charge. Due to the characteristic of the polarization of OAM signal changing with the spatial azimuth angle, some beam displacers (BD) are used to divide the S_{in} signal carrying OAM and SAM information into two vector optical fields (VOF), the W/R beam into two before entering into the atomic cell, and combine two VOF signals into one OAM signal after out of the cell. Here, the topological charge l of the OAM signal S_{in} varies from -5 to 5. The spatial pattern of OAM signal is measured using a camera. The fidelity of OAM and SAM information can be analyzed via a detection system shown in of Fig. 1a.

2.2 AI-optimized memory efficiency

First, we optimize the memory efficiency of single-mode Gaussian signal. To achieve high memory efficiency, a perfect match between signal and control light waveforms is crucial. However, nonlinear waveform matching and the nonlinear response of modulators make the optimization complex and challenging. Although convex optimization and Gaussian approximations can provide quick approximate solutions for certain cases, such as input signals with Gaussian temporal shape, they fall short when it comes to arbitrary waveforms. For practical quantum networks, the optimization method should be adapt to any input waveform, ensuring optimal performance across a wide range of conditions. The existing algorithms face slow convergence and the problem of getting stuck in local minima when searching for the optimal waveform in a vast search space, limiting their practicality. To address these challenges, we develop a waveform optimization method based on a modified DE algorithm using Chebyshev sampling. This approach leverages the roots of Chebyshev polynomials to generate a series of non-uniformly distributed sampling points, which are then used to construct a high-precision approximation of the original function. Compared to traditional equidistant sampling, it achieves a more accurate function approximation with a reduced number of sampling points, especially in areas where the function undergoes rapid changes. By employing this method shown in Fig. 1c, we can significantly reduce the complexity of the parameter space and, through the use of convex optimization algorithms, quickly converge to an approximate optimal solution. This enables high-precision waveform optimization for arbitrary input signals in a relatively short time.

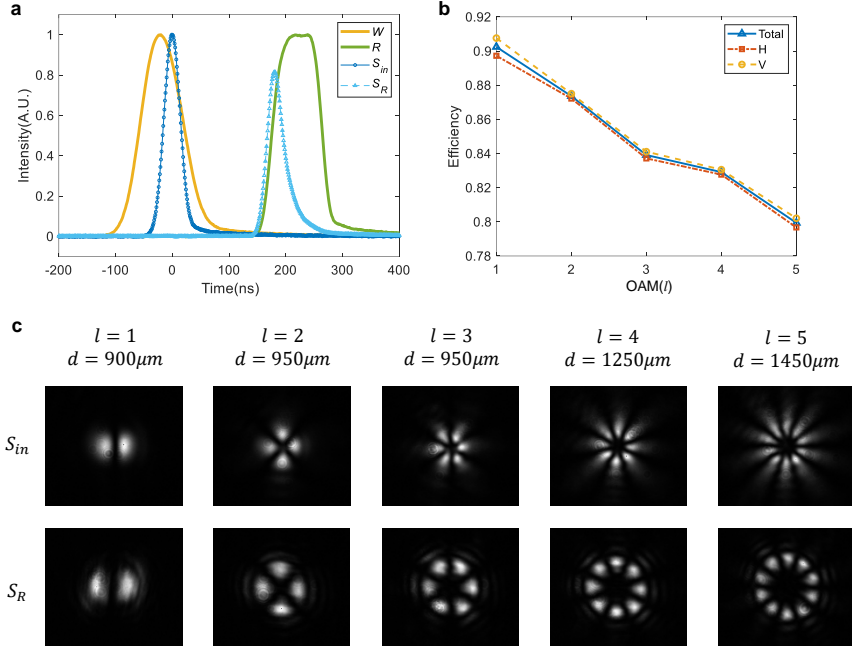


Fig. 2 Experimental efficiency of hyper-dimensional broadband memory. (a) Temporal waveforms of the input signal (S_{in} , yellow), write (W , blue), the retrieved signal (S_R , purple) and read (R , red) pulses in one-time memory. The FWHM of the S_R signal pulse is 20 ns, corresponding to a bandwidth of 50 MHz. (b) Memory efficiency as a function of topological charge l of OAM, the blue triangle is the overall efficiency, the orange square and yellow circle represent the horizontal and vertical polarization path, respectively. (c) The spatial patterns of S_{in} at the center of the atomic cell and S_R with topological charge l from 1 to 5.

Then, we measure memory efficiency of hyper-dimensional signals. Fig. 2b shows the efficiency of different OAM modes. In the case of topological charge $l=1,-1$, efficiency can reach 91%, while gradually drops to 80% at $l=5,-5$. The decrease of η_M is resulted from the increase of the beam waist as l . The beam waist ω of the OAM mode is $\omega = \sqrt{l+1}\omega_0$, where ω_0 is the Gaussian beam waist. The beam waist and central singular point both increase as l , which is clearly shown in Fig. 2c. Larger waist of S_{in} requires larger diameter of the W beam leading to a decrease in the light density, resulting in a reduction in atom-light coupling strength. This is the main reason for efficiency decrease of higher-order OAM optical fields. Therefore, reducing the beam waist of the OAM signal and the W beam using lens is the effective way to increase the coupling coefficient and improve memory efficiency. However, smaller diameter and larger topological charge also simultaneously reduces the number of the effective atoms, which in turn leads to a weakening of the coupling strength. Ultimately, the memory efficiency is the result of optimal coupling determined by both the number of atoms and the waist of optical fields. As shown in Fig. 2b, after optimizing the spot size of OAM signal, the decline rate of memory efficiency is greatly alleviated.

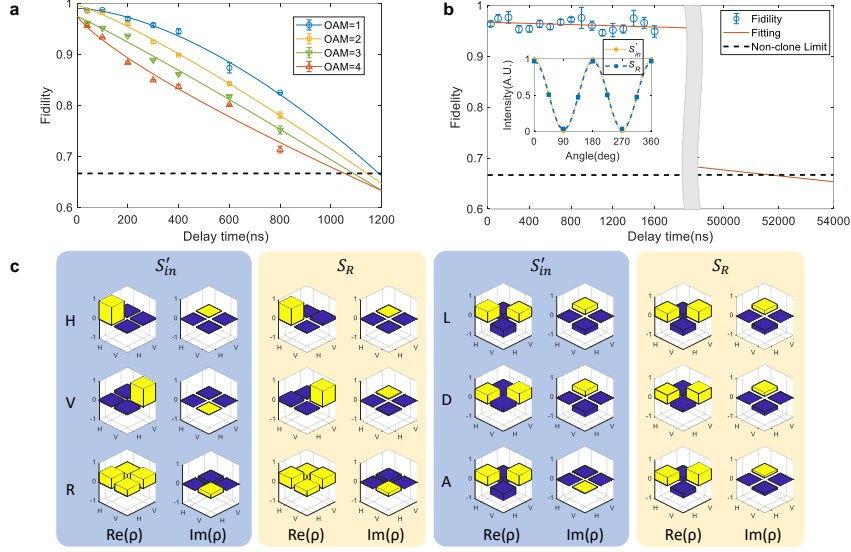


Fig. 3 Fidelity as a function of the delay time for OAM (a) and SAM (b). The delay time is the time difference between the W and R pulses. The inset of (b): intensity of horizontal polarization of before and after memory as the polarization angle changes from 0 to 2π . (c) The projection results of SAM information of S'_{in} and S_R signals for $l = 1$. S'_{in} is the S_{in} signal passing through the whole optical path without memory by blocking pump field.

2.3 Fidelity

Fidelity is the core criterion for judging whether it is quantum memory. The fidelity values for the SMG signal, OAM and SAM information are measured and given in Fig. 3. Benefited from high efficiency and low noise, the memory fidelity of SMG is achieved up to 99%, which is calculated via $F(\rho_{in}, \rho_R) = \text{Tr}[\sqrt{\sqrt{\rho_{in}}\rho_R\sqrt{\rho_{in}}}]$ [21] based on the density matrix ρ_{in} and ρ_R of S_{in} and S_R measured using homodyne detection. Fig. 2c shows the spatial patterns of the OAM signals, S_{in} and S_R . By counting the number of light spots in the spatial patterns of the S_{in} and S_R signals, we can achieve integer-order OAM information. From the patterns in Fig. 2c, the topological number of the OAM pattern l is 1-5 from left to right. By analyzing the azimuth angle of the input and output optical field spatial patterns through image recognition, we can obtain azimuth angle shift and fidelity of the OAM memory. After a delay time of 30 ns, the azimuth angle shift of the OAM spatial pattern is smaller than 10^{-2} rad for $l=1$ and 10^{-3} rad for $l=4$, showing that current atomic memory can store the spatial patterns information of OAM signal well.

The memory fidelity of OAM information is the similarity of the spatial distributions between S_{in} and S_R signals. We perform circular sampling on the OAM spatial pattern image in Fig. 2c to obtain the intensity distribution with spatial angle, and then, operate fast Fourier transform to obtain the phase spectra of the S_{in} and S_R with same topological charge, which are two one-dimensional vectors V_{in} and V_R . The fidelity of OAM information can be obtained by calculating the similarity between

these two vectors $F = (V_{in} \cdot V_R) / (|V_{in}| \times |V_R|)$ [22]. The results are given in Fig. 3a. The fidelity is 96%~98% when delay time $\tau=30$ ns, which are far beyond the no-cloning limitation (67%)[23], indicating that current OAM memory is quantum one. Fig. 3a shows the fidelity of OAM as a function of delay time between the W and R pulses. The fidelity decrease with the topological charge and delay time. We define the memory time for OAM information is the delay time when the fidelity decrease to 67%. The memory time is shortest 1.04 μ s for $l = 4$ and longest 1.2 μ s for $l = 1$, corresponding time-bandwidth product of 52 and 60. In current memory, the diffusion due to atomic thermal motion is the main impact factor on the memory time of OAM spatial patterns. Our experimental results show that the higher order of OAM, the larger affect by diffusion.

According to Fig. 2b, memory efficiency of the OAM information decreases with the topological charge even after optimizing the spot size. Therefore, efficiency for high-order OAM signal may be very low. This is also why SAM information is encoded with the OAM, which can ensure both high dimensionality and high memory efficiency. In experiment, when the OAM mode is encoded on the S_{in} signal by VPP, the SAM information can be simultaneously encoded on S_{in} signal using wave plates (HWP, QWP) as Fig. 1a shown. After the signals are read out as S_R , they are converted back to polarization states by a second VPP plate in the detection optical path. The SAM encoded on signal introduces two more dimensions orthogonal to the OAM, namely the horizontal and vertical polarization (H, V). By combining H and V polarization, SAM information can be added on the OAM. Such operation expands the dimension number from 11 ($l=-5\sim 5$) to 22.

The fidelity of SAM information is measured and given in Fig. 3b. Before measuring the memory fidelity, we need to assess the impact of optical components in the signal propagation path on SAM information. We qualify it by the visibility of S_{in} and S'_{in} as the inset of Fig. 3b shown, which is respective 99% and 93%, showing that the optical components in the optical path cause a certain degree of damage to the fidelity of SAM information. S'_{in} is the S_{in} signal passing through the whole optical path without memory by blocking pump field. Then the memory fidelity of the SAM information is measured and analyzed by comparing the S_{in} and S_R signals. By using QWP and HWP, we can obtain six polarization states, that is, $|H\rangle = |0\rangle$ and $|V\rangle = |1\rangle$, $|D\rangle = |0\rangle + |1\rangle$ and $|A\rangle = |0\rangle - |1\rangle$ by adding a polarization angle of 45° via HWP, $|R\rangle = |0\rangle + i|1\rangle$ and $|L\rangle = |0\rangle - i|1\rangle$ by adding a phase difference of $\pi/2$ via QWP.

We measured six polarization projections of S'_{in} and S_R signals to experimentally reconstruct the density matrix of the polarization states by quantum state tomography (QST) performed using a combination of a quarter-wave plate, a half-wave plate, PBS and photo-detector modules as shown in Fig. 1a. This fidelity reflects the preservation of SAM information during the memory process, without considering the influence of optical components on SAM information. The density matrix results for the six polarization states are shown in Fig. 3c. Based on the density matrices $\rho_{S_{in}}$ and ρ_{S_R} , we obtained the fidelity values. The memory fidelity for six polarizations ($|H\rangle$, $|V\rangle$, $|R\rangle$, $|L\rangle$, $|D\rangle$ and $|A\rangle$) are 98.9%, 97.4%, 99.5%, 98.3%, 99.3%, and 97.6%, respectively. All are far beyond no-cloning limitation 67%. Fig. 3b gives average polarization fidelity F as a function of the memory time τ . The memory time is $\sim 50\mu$ s, which is much longer

than that of OAM one. We achieve high-fidelity SAM memory. For signal carrying both OAM and SAM, the final memory time depends on the shorter one, yielding a 1.0 microsecond memory time for current super-dimensional memory.

3 Discussion

We have demonstrated a hyper-dimensional and high bandwidth quantum memory in an ^{87}Rb atomic vapor cell with efficiency of 91%, bandwidth of 50MHz, the fidelity of the OAM and SAM information up to 96%. This is the highest efficiency to date for both high bandwidth and dimensional quantum memory. In this paper, we generate 22 dimensions corresponding to 66 states through the direct product of OAM and SAM states, and have experimentally achieved high-efficiency, high-fidelity broadband quantum memory for these states. In the future, by hybrid encoding OAM and SAM information in superposition states, we can expand the number of high-dimensional states, while maintaining the same memory efficiency as currently achieved. Our works undoubtedly provide strong support for the realization of large-scale and high-speed quantum networks.

4 Methods

4.1 Frequency control of the optical field

This experiment requires a high-intensity control optical field that satisfies the wave vector matching condition. According to the atomic energy level diagram shown in Figure 1b, there is a frequency $\Delta + \Delta_R$ difference between S_R and S_{in} , which are the single-photon detuning of the write and read light, respectively. They are 1.8 GHz and 1.7 GHz under optimal conditions, so the frequency difference between S_R and S_{in} is 3.5 GHz. In order to obtain the local oscillator optical field corresponding to the frequency S_R , the initial optical field needs to be down-shifted by 3.5 GHz. Through the above processing, this experiment obtained the required signal light pulse and local oscillator light field. However, due to the sensitivity of memory process to the two-photon resonance condition, it is necessary to stabilize the write light frequency at the signal two-photon resonance frequency $\Delta_{hf} + \Delta_{AC}$, where Δ_{hf} is the frequency difference between the atomic energy levels $|g\rangle$ and $|m\rangle$ of 6.834 GHz. The dynamic change Δ_{AC} caused by the AC stark effect of the control light field needs to be adjusted in real time according to the storage effect during the experiment. In order to achieve stable frequency output, an optical phase-locked loop is used to lock the frequencies of two lasers in the experiment.

4.2 The flowchart of AI algorithm

To find the best waveform parameter $\Omega(t)$ for W pulse. The Chebyshev sampling differential evolution algorithm initiates by determining the degree of Chebyshev polynomial to calculate the corresponding time nodes t_j . An first population $\Omega(t_j^1)$ is randomly generated, followed by non-linear interpolation at the Chebyshev nodes to create smooth waveform functions $\Omega_j^1(t)$ and feedback it to acoustic optic modulator

to experimentally output the waveform of W pulse. The corresponding leaking signal $S_{L,j}^1(t)$ is recorded and feedback into the DE algorithm. The algorithm calculate memory efficiency η_j^1 for waveform $\Omega_j^1(t)$ and applies differential evolution operations to refine the population $\Omega(t_j^1)$. This process continues until a convergence criterion is met, at which point the waveform parameters $\Omega(t_j^k)$ that maximize efficiency are identified as the optimal solution. Experimentally, a coherent S_{in} signal is used with 20ns-long Gaussian temporal shape and single-mode Gaussian spatial mode. As shown in Fig. 1d, the memory efficiency of the S_{in} signal is stably achieved to 92%, which support efficient quantum memory of hyper-dimensional signal well. Fig. 2a shows the temporal waveform of the input S_{in} pulse, optimized W pulse, the R pulse and retrieved S_R signal.

Data availability

All relevant data and figures supporting the main conclusions of the document are available on request. Please refer to Liangyu Chen at liangyuc@chalmers.se.

Code availability

All relevant code supporting the document is available upon request. Please refer to Liangyu Chen at liangyuc@chalmers.se.

Funding

This work is supported by the National Natural Science Foundation of China Grants No. U23A2075, No. 12274132, No. 11904227, No. 12104161, No. 12304391 and No. 11974111; Fundamental Research Funds for the Central Universities; the China Postdoctoral Science Foundation (Grant No. 2023M741187, No. GZC20230815), and Innovation Program of Shanghai Municipal Education Commission No. 202101070008E00099.

Author contribution

Z.L. performed the measurements and analysis of the results. Z.L. and J.G. designed the device. Z.L., Z.Y. and H.W. contributed to the implementation of the experimental system. L.Q.C., C.Y., Z.L., Z.Y. and J.G. developed the idea and carried out theoretical simulations of the system. Z.L. and J.G. developed the artificial intelligent algorithm. Z.L., L.Q.C., J.G. and Z.Y. wrote the manuscript. Z.L., L.Q.C., C.Y., H.W. and W.Z. edited the manuscript. L.Q.C. provided supervision and guidance during the project. All authors contributed to the discussions and interpretations of the results.

Competing interests

The authors declare no competing interests.

References

- [1] Cory, D. G., Fahmy, A. F. & Havel, T. F. Ensemble quantum computing by nmr spectroscopy. *Proceedings of the National Academy of Sciences* **94**, 1634–1639 (1997).
- [2] Kielpinski, D., Monroe, C. & Wineland, D. J. Architecture for a large-scale ion-trap quantum computer. *Nature* **417**, 709–711 (2002).
- [3] Zhong, H.-S. *et al.* Quantum computational advantage using photons. *Science* **370**, 1460–1463 (2020).
- [4] Kok, P. *et al.* Linear optical quantum computing with photonic qubits. *Reviews of modern physics* **79**, 135 (2007).
- [5] Bhaskar, M. K. *et al.* Experimental demonstration of memory-enhanced quantum communication. *Nature* **580**, 60–64 (2020).
- [6] Chen, Y.-A. *et al.* An integrated space-to-ground quantum communication network over 4,600 kilometres. *Nature* **589**, 214–219 (2021).
- [7] Hu, X.-M., Guo, Y., Liu, B.-H., Li, C.-F. & Guo, G.-C. Progress in quantum teleportation. *Nature Reviews Physics* **5**, 339–353 (2023).
- [8] Kimble, H. J. The quantum internet. *Nature* **453**, 1023–1030 (2008).
- [9] Sangouard, N., Simon, C., De Riedmatten, H. & Gisin, N. Quantum repeaters based on atomic ensembles and linear optics. *Reviews of Modern Physics* **83**, 33–80 (2011).
- [10] Usmani, I., Afzelius, M., De Riedmatten, H. & Gisin, N. Mapping multiple photonic qubits into and out of one solid-state atomic ensemble. *Nature Communications* **1**, 12 (2010).
- [11] Lan, S.-Y. *et al.* A multiplexed quantum memory. *Optics express* **17**, 13639–13645 (2009).
- [12] Sinclair, N. *et al.* Spectral multiplexing for scalable quantum photonics using an atomic frequency comb quantum memory and feed-forward control. *Physical review letters* **113**, 053603 (2014).
- [13] Pu, Y. *et al.* Experimental realization of a multiplexed quantum memory with 225 individually accessible memory cells. *Nature communications* **8**, 15359 (2017).
- [14] Ding, D.-S. *et al.* Toward high-dimensional-state quantum memory in a cold atomic ensemble. *Physical Review A* **90**, 042301 (2014).

- [15] Ding, D.-S. *et al.* Quantum storage of orbital angular momentum entanglement in an atomic ensemble. *Physical review letters* **114**, 050502 (2015).
- [16] Cao, M., Hoffet, F., Qiu, S., Sheremet, A. S. & Laurat, J. Efficient reversible entanglement transfer between light and quantum memories. *Optica* **7**, 1440–1444 (2020).
- [17] Wang, C. *et al.* Efficient quantum memory of orbital angular momentum qubits in cold atoms. *Quantum Science and Technology* **6**, 045008 (2021).
- [18] Dong, M.-X. *et al.* Highly efficient storage of 25-dimensional photonic qudit in a cold-atom-based quantum memory. *Physical Review Letters* **131**, 240801 (2023).
- [19] Guo, J. *et al.* High-performance raman quantum memory with optimal control in room temperature atoms. *Nature communications* **10**, 148 (2019).
- [20] Yao, A. M. & Padgett, M. J. Orbital angular momentum: origins, behavior and applications. *Advances in optics and photonics* **3**, 161–204 (2011).
- [21] Nielsen, M. A. & Chuang, I. L. *Quantum computation and quantum information* (Cambridge university press, 2010).
- [22] Xia, P., Zhang, L. & Li, F. Learning similarity with cosine similarity ensemble. *Information sciences* **307**, 39–52 (2015).
- [23] Grosshans, F. & Grangier, P. Quantum cloning and teleportation criteria for continuous quantum variables. *Physical Review A* **64**, 010301 (2001).